

PHYSICAL REVIEW D

PARTICLES AND FIELDS

THIRD SERIES, VOLUME 30, NUMBER 5

1 SEPTEMBER 1984

Pion pair production from $\gamma\gamma$ collisions at the SLAC e^+e^- storage ring PEP

J. R. Smith,^a D. L. Burke, A. M. Boyarski, M. Breidenbach, J. M. Dorfan, G. J. Feldman
L. Gladney, G. Hanson, R. J. Hollebeck, W. R. Innes, J. A. Jaros, A. J. Lankford, R. R. Larsen, B. LeClaire,
N. Lockyer, V. Lüth, C. Matteuzzi, M. L. Perl, B. Richter, D. Schlatter,^b J. Weiss,^c
J. M. Yelton, and C. Zaiser

Stanford Linear Accelerator Center, Stanford University, Stanford, California 94305

G. S. Abrams, D. Amidei, W. Chinowsky, W. E. Dieterle,^d J. B. Dillon,^e M. W. Eaton,^f M. E. B. Franklin,
G. Gidal, M. S. Gold, G. Goldhaber, L. J. Golding, A. D. Johnson,^g J. A. Kadyk, M. E. Nelson,^h
J. F. Patrick,ⁱ P. C. Rowson, H. M. Schellman, P. D. Sheldon, J. Strait,^j and C. de la Vaissière
Lawrence Berkeley Laboratory and Department of Physics, University of California, Berkeley, California 94720

C. A. Blocker, M. Levi,^b T. Schaad, and R. F. Schwitters

Department of Physics, Harvard University, Cambridge, Massachusetts 02138

(Received 6 February 1984)

We have studied several features of the production of charged-hadron pairs by $\gamma\gamma$ collisions. We have measured the f^0 partial width $\Gamma_{f^0 \rightarrow \gamma\gamma}(Q^2)$ for Q^2 in the range $0 < Q^2 < 1.4 \text{ GeV}^2/c^2$, and obtained $\Gamma_{f^0 \rightarrow \gamma\gamma} = 2.52 \pm 0.13 \pm 0.38 \text{ keV}$ at $Q^2 \approx 0$. The measured Q^2 dependence is in agreement with the generalized vector-dominance model. The cross section for $\gamma\gamma \rightarrow (\pi^+\pi^- + K^+K^-)$ in the mass region $1.6 \leq M_{\pi\pi} \leq 2.5 \text{ GeV}/c^2$ has also been measured and the result compared with that expected from the QCD continuum.

I. INTRODUCTION

We have studied the $\gamma\gamma$ process, $e^+e^- \rightarrow e^+e^- + 2$ charged prongs, with the MARK II detector at the e^+e^- storage ring PEP. In particular, we have measured the partial width of the $f^0(1270)$, and also measured the hadron-pair-production rate in the region of higher masses $1.6 < M_{\pi\pi} < 2.5 \text{ GeV}/c^2$. When the incident beam leptons are not observed in the final state the event is said to be *untagged* and both of the photons involved have negligible Q^2 . A measurement of the untagged production cross section $\sigma(\gamma\gamma \rightarrow f^0)$ provides a value for $\Gamma_{f^0 \rightarrow \gamma\gamma}$ at $Q^2 \approx 0$. Events in which one of the outgoing beam leptons is detected are said to be *single tagged* and provide a measurement of the Q^2 dependence of the production cross section. We have studied both single-tagged and untagged production of the $f^0(1270)$ and have made comparisons of our results with various theoretical models. Perturbative QCD predictions¹ have been made for the $\gamma\gamma \rightarrow \pi^+\pi^-$ and $\gamma\gamma \rightarrow K^+K^-$ processes at high invariant mass, and we compare these with our measurements of untagged hadron pairs with $M_{\pi\pi} > 1.6 \text{ GeV}/c^2$.

Production of the $f^0(1270)$ by two real ($Q^2 \approx 0$) photons has been studied by many groups, including the MARK II and Crystal Ball collaborations at SPEAR, and

the TASSO, PLUTO, JADE, and CELLO collaborations at PETRA. The value of the partial width $\Gamma_{f^0 \rightarrow \gamma\gamma}$ found in the latest Particle Data Group tables² is $2.86 \pm 0.05 \text{ keV}$. The TASSO³ collaboration has measured the production of the f^0 in the tagged mode with $Q^2 \approx 0.35 \text{ GeV}^2/c^2$ and has found that the partial width, extrapolated to $Q^2 = 0$ with a form factor given by Ref. 4, is $1.6 \pm 0.6 \pm 0.3 \text{ keV}$, which is smaller than the value of $\Gamma_{f^0 \rightarrow \gamma\gamma}$ that they report for the untagged case. The PLUTO⁵ collaboration has placed an upper limit $\Gamma_{f^0 \rightarrow \gamma\gamma} < 2.6 \text{ keV}$ for a range of Q^2 similar to the TASSO range. A measurement of the double-tagged production of the f^0 made at SPEAR⁶ obtained a partial width of $9.5 \pm 3.9 \pm 2.4 \text{ keV}$ for Q^2 values of each virtual photon in the range $0.07 - 0.3 \text{ GeV}^2/c^2$. Measurements of the cross section for $\gamma\gamma \rightarrow (\pi^+\pi^- + K^+K^-)$ at masses below $\approx 1.5 \text{ GeV}/c^2$ have been made by the MARK II group at SPEAR.⁷ The cross section in this mass was found to be consistent with that expected from the Born amplitude for pointlike pions and the $f^0(1270)$ meson. In this paper we report measurements of $\sigma(\gamma\gamma \rightarrow \pi^+\pi^-) + \sigma(\gamma\gamma \rightarrow K^+K^-)$ at masses above the $f^0(1270)$ and make comparisons with predictions from perturbative QCD calculations.

In the following sections we discuss the results of the present measurements. Section II contains a brief descrip-

tion of the central part of the MARK II detector. Section III describes the apparatus used to detect electrons scattered at small angles with respect to the beam direction. In Secs. IV and V, we present discussions of the untagged and tagged data respectively.

II. CENTRAL DETECTOR

The MARK II central detector, shown in Fig. 1, has been previously described in detail.^{8,9} Charged-particle tracking is accomplished with multilayer cylindrical drift chambers centered in a 2.3-kG solenoidal magnet. The momentum resolution of the spectrometer is

$$\Delta p/p = [(0.02)^2 + (0.0095p)^2]^{1/2} \quad (p \text{ in GeV}/c)$$

for tracks constrained to the beam intersection point (IP). This momentum resolution is more than sufficient for the purpose of the work presented in this paper. The minimum momentum required for a particle to traverse all of the drift-chamber layers is 100 MeV/c, and the detector is triggered on events that have at least two particles with momentum greater than this value and angles to the beam direction (θ) greater than 45° . The momentum cutoff causes no problem for the detection of the f^0 , since the momentum distribution for the $\pi^+\pi^-$ from the decay of the f^0 peaks around 600 MeV/c, and the probability that an individual pion has a momentum less than 100 MeV/c from such a decay is very small (less than 0.2%). A time-of-flight (TOF) system, consisting of scintillation counters at a radius of 1.5 m, measures flight times with a resolution of ~ 320 psec for particles with $|\cos\theta| < 0.76$. The TOF system is part of the charged-particle trigger and is also used to reject cosmic rays and identify protons below a momentum of 2 GeV/c. Electromagnetic showers are identified with an energy resolution of $\sigma_E \approx 14\% \sqrt{E}$ (energy in GeV) using eight lead-liquid-argon (LA) calorimeter modules. The LA system covers the region $|\cos\theta| < 0.7$ and is used to separate electrons from hadrons at momenta above 600 MeV/c. Muons of momenta ≥ 750 MeV/c are identified over 55% of 4π steradians with four layers of iron absorber interleaved with proportional tubes.

III. SMALL-ANGLE TAGGER

One arm of the small-angle tagging (SAT) system is shown in Fig. 2. A detailed description of this hardware can be found in Ref. 10; here we give a brief sketch of the

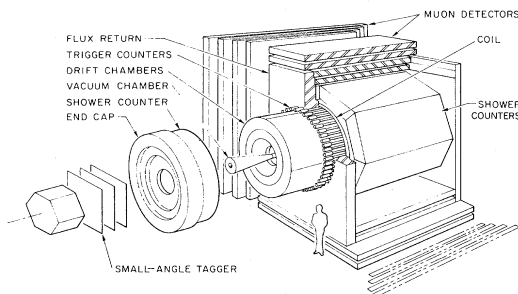


FIG. 1. Isometric view of the MARK II central detector.

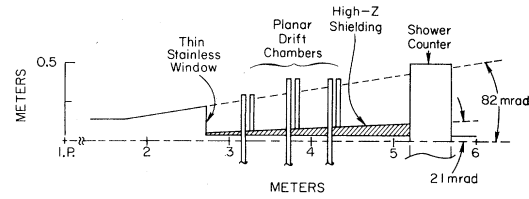


FIG. 2. The small-angle tagging system.

apparatus. It consists of three sets of four planar drift chambers and a pair of electromagnetic shower counters. These drift chambers and shower counters cover the polar angles between 21 and 82 mr from the beam axis. It would also be possible to tag electrons in the central detector (20° to 160°), but the rate is too low to be useful for the present study of the f^0 .

Each plane of drift chambers is arranged around the beam pipe in a rectangular array with two vertical chambers and two horizontal chambers. The spatial resolutions of these chambers is $\approx 300 \mu\text{m}$ in the drift coordinate, and a delay line under each sense wire provides a measurement of the orthogonal coordinate with a resolution of ≈ 0.5 cm. In the region of overlap (i.e., the corners), one obtains good resolution in both the x and y coordinates which are orthogonal to the beam direction. The accuracy of the measurement of the track's slope and intercept depends on the number of x and y hits made by the track in the drift chambers and also on random-noise hits assigned to the track. Each reconstructed track was projected backward along the beamline to the x - y plane at the z position of the IP, and all tracks that project radially to within 3 cm of the IP were used in the analysis presented here. Since well-measured tracks are more likely to have a small intercept at the IP x - y plane than poorly measured tracks, the acceptance in the regions where the x and y chambers overlap is better than in the nonoverlap region where only one coordinate is measured well. The efficiency in the overlapping sections of the chambers was determined to be $96 \pm 0.5\%$ from a study of Bhabha events and checked with a Monte Carlo simulation that used the EGS electromagnetic-shower code.¹¹ The efficiency in the nonoverlapping sections was determined to be $58 \pm 5\%$ by taking the ratio of the accepted events in the nonoverlapping sections to those in the corners, suitably correcting for the difference in solid angle, and then multiplying by the measured efficiency in the corners.

The electromagnetic-shower-counter modules are constructed of sandwiches of 0.63-cm lead sheets and 1.27-cm NE114 plastic scintillators. There are 18 layers each of lead and scintillator. Wave-shifter bars (BBQ) are used to transmit light from the scintillators to standard 44-mm photomultiplier tubes. The energy resolution of these shower counters was measured with Bhabha events and found to be $\sigma_E = 15.5\% \sqrt{E}$. The first five layers of the shower counter are read out together and the last 13 layers are read out together.

IV. RESULTS FROM THE UNTAGGED DATA

For the untagged data, we demanded that just two charged prongs with opposite charges be found in the cen-

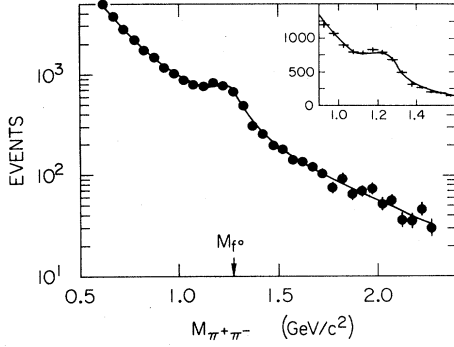


FIG. 3. Observed untagged $\gamma\gamma \rightarrow 2$ prong mass spectrum (14.5 pb^{-1}). The curve is the result of a fit described in the text. The inset shows the result of the fit on a linear scale in the mass region around the f^0 .

tral detector. The detected pair was required to form a vertex with position coordinate along the beam axis within 6 cm of the IP, and radial distance from the beam axis less than 3 cm. Each prong was required to be within the region $|\cos\theta| < 0.7$ to eliminate uncertainties in the acceptance of the trigger logic. Cosmic-ray events were rejected by time-of-flight measurements. Protons and pions with momenta $p \leq 1 \text{ GeV}/c$ are well separated by time of flight and so events with either prong identified as a proton were removed. Since the momenta of the pions from the f^0 are typically around $600 \text{ MeV}/c$, the muon system was not used, and electron separation with the liquid-argon system was not attempted because of the rapidly varying electron detection efficiency in this region. To eliminate beam-gas background and also contamination from higher multiplicity states the total transverse momentum of the pair was required to be less than $100 \text{ MeV}/c$. This requirement effectively limits the Q^2 of the accepted events to less than $0.04 \text{ GeV}^2/c^2$. Figure 3 shows the mass plot obtained with these selection criteria from an integrated luminosity of 14.5 pb^{-1} at a beam energy of 14.5 GeV . All the prongs were assumed to be pions. This two-prong sample is dominated by the QED processes $e^+e^- \rightarrow e^+e^-e^+e^-$ and $e^+e^- \rightarrow e^+e^-\mu^+\mu^-$. However, one can distinctly see the f^0 resonance in the data.

Data from SPEAR⁷ indicate that, in addition to the f^0 , there is nonresonant pion production in the mass region shown in Fig. 3. This nonresonant pion contribution can interfere with the resonant pion component. A fit to the data in Fig. 3 was performed using a Monte Carlo calculation of the QED mass shape¹² and also a model for the pion mass spectrum. This model allows for interference between the f^0 resonance and the continuum by using a relative phase shift between the two channels given by the angle δ where

$$\tan\delta(M_{\pi\pi}) = \frac{M_{f^0}\Gamma_{\text{tot}}}{M_{f^0}^2 - M_{\pi\pi}^2}.$$

The pion cross section was assumed to have the form⁷

$$\begin{aligned} \frac{d\sigma}{d\Omega^*}(\gamma\gamma \rightarrow \pi\pi) &= Ah(M_{\pi\pi}) + \Gamma_{f^0 \rightarrow \gamma\gamma} g(M_{\pi\pi}) + f'(M_{KK} \rightarrow M_{\pi\pi}) \\ &+ 2B \cos\delta(M_{\pi\pi}) [\Gamma_{f^0 \rightarrow \gamma\gamma} Ah(M_{\pi\pi}) g(M_{\pi\pi})]^{1/2}. \end{aligned} \quad (1)$$

Here $h(M_{\pi\pi})$ represents the pion-continuum mass shape which was chosen to be a combination of the Born cross section and the QCD cross section.¹ The Born term was assumed to be valid for $M_{\pi\pi}$ below $1 \text{ GeV}/c^2$ and QCD valid for $M_{\pi\pi}$ above $1 \text{ GeV}/c^2$. These are approximately equal at $M_{\pi\pi} = 1 \text{ GeV}/c^2$, so the normalization of the QCD shape was adjusted to make them equal at $1 \text{ GeV}/c^2$ and the parameter A was then used in the fit described below. The function $g(M_{\pi\pi})$ contains the relativistic Breit-Wigner line shape of the f^0 and also the assumed helicity-2 angular distribution. It is given by

$$\begin{aligned} g(M_{\pi\pi}) &= \frac{8\pi^2(2J+1)}{M_{\pi\pi}} |Y_{22}|^2 \frac{1}{\pi} \\ &\times \frac{M_{f^0}\Gamma_{\text{tot}}}{(M_{\pi\pi}^2 - M_{f^0}^2)^2 + M_{f^0}^2\Gamma_{\text{tot}}^2} B_{f^0 \rightarrow \pi^+\pi^-}. \end{aligned} \quad (2)$$

Here Γ_{tot} is the effective resonance total width which has mass dependence due to the centrifugal potential:¹³

$$\Gamma_{\text{tot}}(M_{\pi\pi}^2) = \Gamma_{f^0} \left[\frac{q(M_{\pi\pi}^2)}{q(M_{f^0}^2)} \right]^{2J+1} \frac{D_2(q(M_{\pi\pi}^2)r_{f^0})}{D_2(q(M_{f^0}^2)r_{f^0})}, \quad (3)$$

where

$$q(s) = (s/4 - m_\pi^2)^{1/2}$$

and

$$D_2(z) = (9 + 3z^2 + z^4)^{-1}.$$

In the above we have taken the following constants appropriate for the f^0 meson:

$$J = 2,$$

$$r_{f^0} = 1 \text{ fm} = 5.068 (\text{GeV}/c)^{-1},$$

$$\Gamma_{f^0} = 0.180 \text{ GeV},$$

$$M_{f^0} = 1.270 \text{ GeV}/c^2,$$

and

$$B_{f^0 \rightarrow \pi^+\pi^-} = \frac{2}{3} \times 0.831.$$

A partial-wave decomposition was not attempted and therefore a parameter B was inserted into the fit. If the continuum and the resonance were in the same partial wave B would be 1. Since kaons were not explicitly eliminated, the two-prong data sample can also contain $f'(1515)$ decays. To correct for this we include a fixed contribution from $f' \rightarrow K^+K^-$ using the partial width¹⁴ $\Gamma_{f' \rightarrow \gamma\gamma} = 0.11 \text{ keV}$. The f^0 produced in the untagged case is known to be predominantly produced in helicity 2.¹⁵ By assuming that the cross section for e^+e^-

$\rightarrow e^+e^-\pi^+\pi^-$ factorizes into a $\gamma\gamma$ cross section multiplied by a $\gamma\gamma$ luminosity function, we can write in the untagged case¹⁶

$$\frac{d\sigma(ee \rightarrow ee\pi^+\pi^-)}{dM d\Omega^*} = \left[\frac{2\alpha}{\pi} \ln \frac{E_{\text{beam}}}{m_e} \right]^2 \frac{f(z)}{M} \frac{d\sigma(\gamma\gamma \rightarrow \pi^+\pi^-)}{d\Omega^*}, \quad (4)$$

where M is the $\pi^+\pi^-$ invariant mass and $z=M/2E_{\text{beam}}$. The function $f(z)$ is the photon-flux density. For untagged processes it is approximately¹⁷

$$f(z) = (2+z^2)^2 \ln \frac{1}{z} - (1-z^2)(3+z^2). \quad (5)$$

The actual formula that we used was taken from a more precise formulation¹⁸ that accounts for the small Q^2 spread of the untagged events. The above model, with $\Gamma_{f^0 \rightarrow \gamma\gamma}$ used as a parameter, was fitted to the data. The normalization of the QED contribution was also allowed to be a free parameter of the fit. The partial width was stepped through a series of values and the remaining parameters varied to minimize the χ^2 at each value of $\Gamma_{f^0 \rightarrow \gamma\gamma}$. The overall minimum χ^2 was found to give $\Gamma_{f^0 \rightarrow \gamma\gamma} = 2.52 \pm 0.13$ keV. At this minimum the normalization of the QED was 92% of that obtained from the measured luminosity, but the equivalent photon approximation used to compute¹⁶ the QED mass shape is known to overestimate the absolute cross section by 10–20%. The fit also gave $B=0.93$. Because of the detector acceptance most of the observed Born cross section is in helicity 2 and so B very near to 1 is a reasonable value. Such a large interference also accounts for approximately half of the 50-MeV shift of the observed mass peak relative to the nominal f^0 mass. The falling photon flux explains the remainder of the observed shift. The value of $\Gamma_{f^0 \rightarrow \gamma\gamma}$ from the fit can be compared with the result of a more approximate analysis in which a straight subtraction of the sidebands was performed using a smooth curve obtained by renormalizing the QED mass shape in the mass region 0.6 to 0.9 GeV/ c^2 . This method gives a value for the partial width of $\Gamma_{f^0 \rightarrow \gamma\gamma} = 2.68 \pm 0.13$ keV in close agreement with the value obtained from the fit.

The errors quoted above are only the statistical uncertainty of the experiment. The major components of the systematic error are the accuracy of the Monte Carlo calculation of the acceptance of the detector and uncertainties in the $\gamma\gamma$ process itself. We have assumed that the $f(1270)$ is produced in the helicity 2 state. There is evidence from the Crystal Ball¹⁵ that this is the case; however, the detector efficiency for the helicity-0 case is approximately half of that for the helicity-2 final state. We also must correct the measured value for the efficiency of the cut at 100 MeV/ c on the total transverse momentum of the detected pair. This was done by using Monte Carlo distributions for the $\gamma\gamma$ -c.m.s. motion that are consistent with the exact calculations¹² for the QED process $ee \rightarrow ee\mu\mu$. This, however, assumes that the Q^2 dependence of the production of the f^0 is the same as that for QED (see Sec. IV). The accumulated luminosity of the

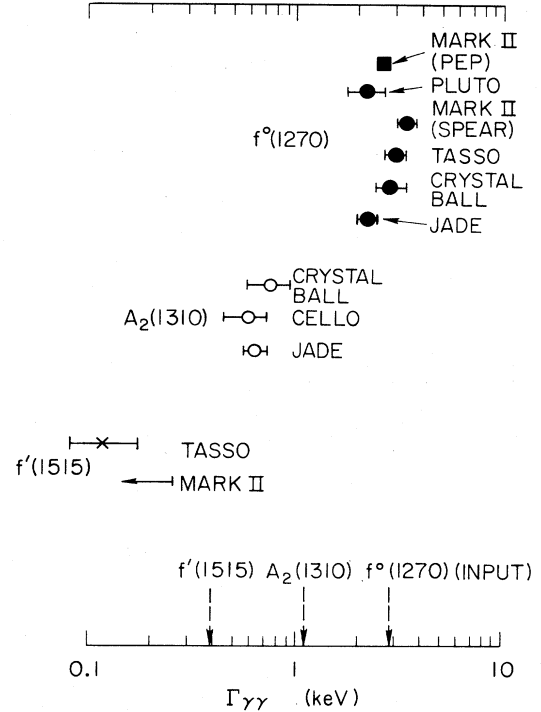


FIG. 4. Summary of measured partial widths of the 2^{++} tensor mesons. Only the reported statistical errors of the measurements are shown. Dashed arrows indicate the phase-space-corrected SU(3) predictions for $\Gamma_{f' \rightarrow \gamma\gamma}$ and $\Gamma_{A_2 \rightarrow \gamma\gamma}$ using the average experimental value of $\Gamma_{f^0 \rightarrow \gamma\gamma}$ as input.

experiment is known to $\pm 3\%$. By assuming these to be uncorrelated errors and adding them in quadrature, we estimate the total systematic error to be 15%. Therefore the value of the partial width we measure is $\Gamma_{f^0 \rightarrow \gamma\gamma} = 2.52 \pm 0.13 \pm 0.38$ keV. This value can be compared with the MARK II SPEAR value of $3.6 \pm 0.3 \pm 0.5$ keV.

Figure 4 shows measured values reported in the literature¹⁹ for the partial widths of the 2^{++} tensor mesons with our new value also shown. Using ideal mixing, this multiplet has the quark assignments

$$\begin{aligned} f &= (u\bar{u} + d\bar{d})/\sqrt{2}, \\ A_2 &= (u\bar{u} - d\bar{d})/\sqrt{2} \\ f' &= (s\bar{s}). \end{aligned}$$

SU(3) symmetry predicts that the $\gamma\gamma$ partial widths of these resonances should be in the ratio of 25:9:2. This SU(3) prediction is shown by the dashed arrows in Fig. 4 using the average value of the f^0 partial width as input and corrected for the different phase space due to the shift in mass of the f' (an m^3 correction was assumed) relative to the other members of this multiplet. The mass splitting itself is evidence that the SU(3) symmetry is only approximate. However, in view of the uncertainty regarding the helicity structure of these reactions, the SU(3) prediction of the partial widths is reasonably close to the data.

Equation (1) can be checked in an independent way. It

makes a prediction for the pion cross section for masses above the f^0 resonance. In this region the liquid argon and muon systems can be used to reject the QED background, thus allowing a direct measurement of cross section $\sigma(\gamma\gamma \rightarrow \text{hadron pairs})$. We have measured $\sigma(\gamma\gamma \rightarrow \text{hadron pairs})$ in the mass region $1.6 \leq M_{\pi\pi} \leq 2.5 \text{ GeV}/c^2$. We demanded $|\cos\theta| < 0.56$ for both tracks, effectively limiting $|\cos\theta^*|$ to be between 0 and 0.3 (θ^* is the angle between the $\gamma\gamma$ axis and the angle of emission of the hadron pair in the $\gamma\gamma$ center-of-mass system). Therefore we present the cross section integrated over the region $|\cos\theta_\pi^*| < 0.3$. The data sample used for this measurement corresponds to an integrated luminosity of 35 pb^{-1} .

The liquid-argon modules measured the shower energy E_{sh} deposited by each prong. Prongs with E_{sh}/p greater than 0.5 were identified as electrons, and events with either track identified as an electron were removed. Events were also removed if either track fell within $\pm 2^\circ$ of a crack between any two of the eight liquid-argon modules. The scatter plot shown in Fig. 5 of E_{sh}/p for one prong versus the other for all two-prong events shows a clean separation between e^+e^- pairs and the remainder of the two-prong sample. From this plot we estimate the probability that both electrons in an e^+e^- pair have E_{sh}/p less than 0.5 to be 0.02%. The muon system was used to reject μ pairs. We checked different ways of cutting on the response of the muon system, and found that the final measured cross sections were not extremely sensitive to the choice of cuts. The first technique was to require that each charged track penetrate fewer layers of steel than would be expected if it were a muon. The second technique was to require that only one charged track have penetrated fewer layers of steel than would be expected for a muon and the other track was not identified as a muon. This accepts some events in which one track falls into the gaps in the azimuthal coverage of the muon sys-

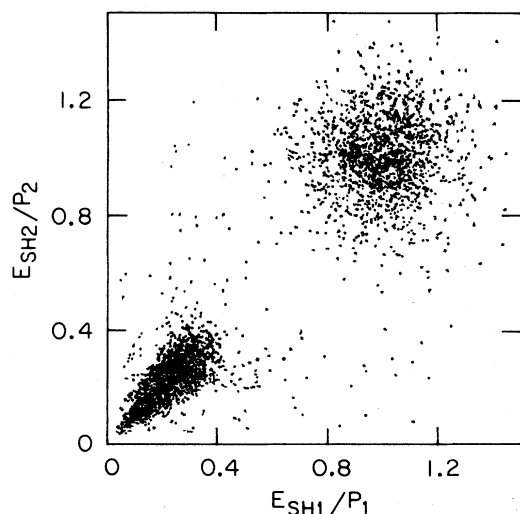


FIG. 5. Scatter plot of the ratio of shower-counter energy to momentum for one prong versus the other in untagged high-mass events.

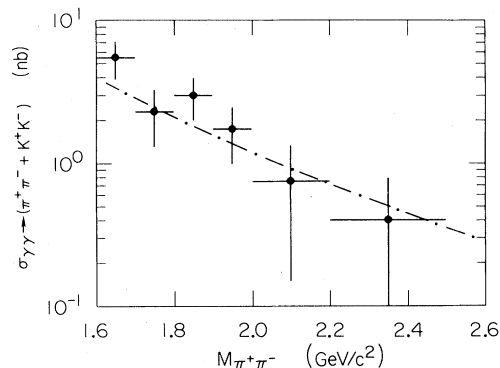


FIG. 6. Measured cross section for $\gamma\gamma \rightarrow \pi^+\pi^-$ plus $\gamma\gamma \rightarrow K^+K^-$ integrated over the angular region $|\cos\theta^*| < 0.3$. The errors contain systematic as well as statistical contributions. The curve is a perturbative-QCD prediction.

tem. In the third technique the analysis was carried out with the more stringent requirement that at least one prong had not penetrated any layers of the muon system while the other prong simply failed to be identified as a muon. Here, as in the second technique, some events are accepted with one prong falling into the azimuthal gaps in the muon system. The data sample with electrons removed was used to make an estimate of the number of μ pair events that are misidentified as hadron pairs by these techniques. Events with one prong identified as a muon were used to determine the probability that the partner is misidentified as a hadron. We find that the misidentification probability for μ pairs is $\approx 0.3\%$ for the first technique, $\approx 1.4\%$ for the second technique, and $\approx 0.3\%$ for the third technique of muon identification. These misidentification probabilities are essentially independent of mass in the region of interest.

The efficiency for pion events to be accepted by the above analysis was computed by Monte Carlo simulation, and was found to be 9.5% for the first and third muon-identification techniques and 11.5% for the second technique. In the mass region 1.6 to 2.5 GeV/c^2 we find 41 events that survive the cuts of the first muon-identification technique, 59 events using the second technique, and 43 using the third technique. The estimated QED background was subtracted bin by bin in the $\pi\pi$ invariant mass to yield the $\gamma\gamma$ cross section shown in Fig. 6. This subtraction ranged from $\approx 10\%$ at 1.6 GeV/c^2 to $\approx 50\%$ at 2.5 GeV/c^2 . The errors shown in the plot include contributions from the uncertainties in the photon flux and pion-pair acceptance, and from the uncertainty in the background subtraction. This latter uncertainty has been estimated from the spread in the results obtained from the different identification techniques described above. Also shown in Fig. 6 is the absolute prediction of a perturbative QCD calculation¹ for pions and kaons with pion masses used throughout. The comparison of the cross section with the QCD prediction indicates agreement in the high-mass region, although the data are statistically limited in this region.

V. RESULTS FROM THE TAGGED DATA

Events with two oppositely charged prongs in the central detector were examined to see if there was a beam lepton detected by the SAT system. Events were kept if a track in the SAT system projected back to within 3 cm of the origin defined by the vertex formed by the charged prongs in the central detector. It was required that the z position of the vertex formed by the two prongs in the central detector be within 7 cm of the IP and the radial distance of this vertex from the beam axis was required to be less than 3.5 cm. As in the untagged case, each of the charged prongs in the central detector region was required to be between 45° and 135° from the beam axis. To isolate tagged $\gamma\gamma \rightarrow 2$ prong events from higher-multiplicity final states we examined the transverse-momentum balance between the tagged electron and the two prongs seen in the central detector. Events with net transverse momentum less than $200 \text{ MeV}/c$ were kept. Figure 7 shows a scatter plot of energy of the tagged electron versus the total visible transverse momentum of the event before the cuts. The tagged energy distribution from $\gamma\gamma$ events peaks near the beam energy and has a long tail extending into the lower-energy region. Below 2 GeV the population rises due to background tracks ($\approx 10\%$ occupancy). Events with tagged electron energy greater than 8 GeV were kept. Also, since Monte Carlo studies indicate that the efficiency for detecting an f^0 falls off rapidly for $|\cos\theta^*_\pi| > 0.8$, events in this range were rejected.

The tagged data were divided into two regions of Q^2 . The first region has Q^2 values extending from 0.05 to $0.26 \text{ GeV}^2/c^2$ and the second region from 0.26 to $1.4 \text{ GeV}^2/c^2$. The resulting mass plots are shown in Fig. 8. The transverse-transverse part of the $\gamma^*\gamma$ cross section, valid for single tagging, is given by^{18,20}

$$\frac{d^5\sigma}{d\omega_1 d\omega_2 d\theta_{\text{tag}} d\Omega^*} = \frac{d^3\mathcal{L}_{TT}(Q^2)}{d\omega_1 d\omega_2 d\theta_{\text{tag}}} \frac{d^2\sigma_{TT}(Q^2)}{d\Omega^*} (\gamma\gamma \rightarrow \pi^+\pi^-). \quad (6)$$

$$\frac{d^3\mathcal{L}_{TT}}{d\omega_1 d\omega_2 d\theta_{\text{tag}}} \approx \frac{\alpha^2}{8\pi^2} K \cot\left[\frac{\theta_{\text{tag}}}{2}\right] \left[\frac{(K-2\omega_1)^2}{K^2} + 1 \right] \times \left[\frac{[K-2(\omega_2+Q_2/4E_b^2)]^2}{K^2} + 1 \right] \ln \left[\frac{2E_b(1-\omega_1)\sin\frac{\hat{\theta}}{2}}{m_e\omega_1} - \frac{2(1-\omega_1)}{\omega_1^2} + \frac{m_e^2}{2E_b^2(1-\omega_1)\sin^2(\hat{\theta}/2)} \right], \quad (7)$$

where E_b is the beam energy and $K = (M_{\pi\pi}^2 + Q^2)/4E_b^2$. Also $\hat{\theta}$ is the minimum tagging angle which is the upper limit in the integration over the untagged electron's polar angle. We have explicitly removed events from our data sample in which *both* beam electrons are detected in the SAT system. In writing expression (6) we have assumed that the Q^2 dependence of the cross-section factors into a part that describes the massive-photon propagator, $\mathcal{L}_{TT}(Q^2)$, and a part that describes the coupling of the photon to the final state, $d\sigma(Q^2)/d\Omega^*$.

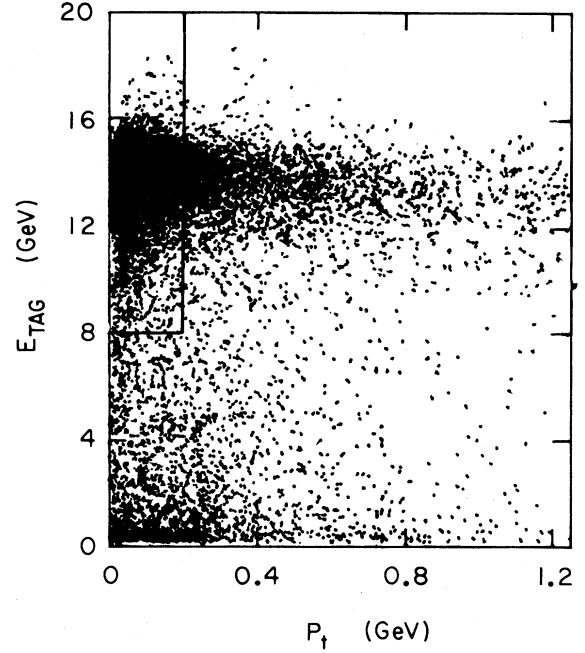


FIG. 7. Scatter plot of tag energy versus net transverse momentum in observed events. The box shows the region in which events were accepted as tagged two-photon events.

Here ω_1 and ω_2 are the untagged and tagged photon total energies, respectively, divided by the beam energy, while θ_{tag} is the angle of the tagged electron. Also, Ω^* is the center of mass solid-angle element of the pion pair. Experimentally one measures the cross section for $e^+e^- \rightarrow e^+e^- + \text{two-charged prongs}$. Equation (6) then forms the basis for converting this cross section into a measurement of the cross section for $\gamma\gamma \rightarrow \text{two charged prongs}$ at nonzero Q^2 . The photon luminosity function, \mathcal{L}_{TT} , is given by

Just as in the untagged case we fit the mass distributions with a QED component and a pion continuum that is allowed to interfere with the resonant $f^0(1270)$. In Fig. 9 we show the Q^2 distribution of the data and compare it with a Monte Carlo calculation¹² of the expected shape of QED processes. We have simply used all events in this figure since the QED completely dominates the mass spectrum. The results of the fits to the two regions of Q^2 are shown in Fig. 8. The total integrated luminosity used for this analysis was also 35 pb^{-1} . The results yield a

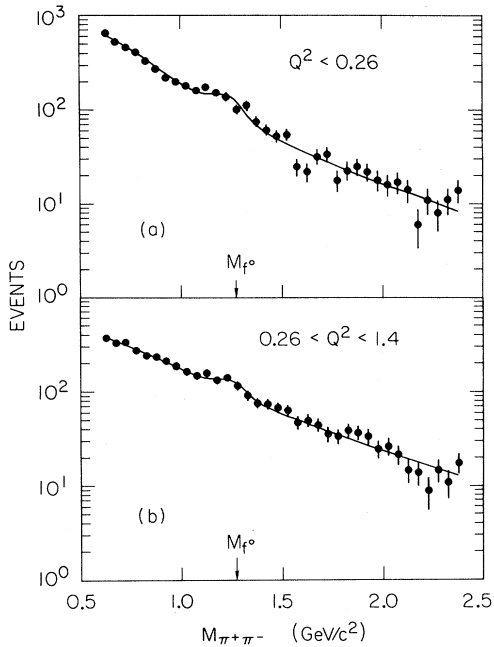


FIG. 8. Single-tagged $\gamma\gamma \rightarrow 2$ prong mass spectrum for $0 < Q^2 < 0.26 \text{ GeV}^2/c^2$ and for $0.26 < Q^2 < 1.4 \text{ GeV}^2/c^2$.

value of the partial width of $1.92 \pm 0.32 \pm 0.39 \text{ keV}$ for $Q^2 < 0.26 \text{ GeV}^2/c^2$ and $1.25 \pm 0.28 \pm 0.27 \text{ keV}$ for $0.26 < Q^2 < 1.4 \text{ GeV}^2/c^2$. We did not measure the center-of-mass angular dependence of the f^0 decay and hence made the assumption for this analysis that it is in the helicity-2 state, just as in the untagged case. Hence, the efficiency for detection of the $\pi^+\pi^-$ pair from the f^0 was determined using angular distributions appropriate for the helicity-2 hypothesis. The major systematic errors are uncertainties in the Monte Carlo calculation of the tagged electron track reconstruction efficiencies, the net transverse-momentum distribution of the $\gamma\gamma$ c.m.s., and the acceptance of the detector. These are each approximately 10%. Also, the uncertainty in the tagged-energy distribution and the modeling of the central detector con-

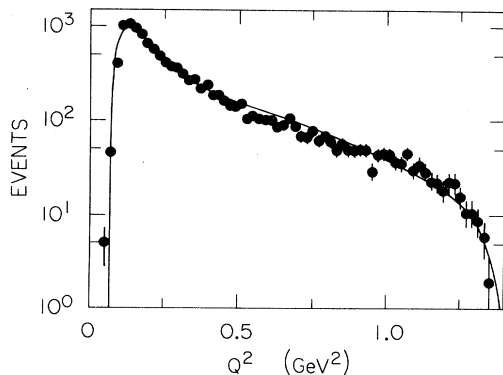


FIG. 9. The Q^2 distribution of the tagged two-prong events compared with a Monte Carlo calculation of the Q^2 dependence of the purely QED processes $ee \rightarrow eeee$ and $ee \rightarrow ee\mu\mu$.

tribute approximately 5% each to the systematic error. Assuming these to be uncorrelated errors and adding them in quadrature gives a resultant systematic error of approximately 20%. The QED normalization from the fits was 93% for $Q^2 < 0.26 \text{ GeV}^2/c^2$ and 108% for $0.26 < Q^2 < 1.4 \text{ GeV}^2/c^2$ of that expected from the measured luminosity and our Monte Carlo program.

The values quoted above for the partial width can be compared with approximate results obtained by using the QED mass shape as a smooth curve through the background. This method entails renormalizing the QED mass shape in the region between 600 and 900 MeV/c^2 and subtracting the renormalized QED component in the mass region 1000 to 1500 MeV/c^2 . The results of this subtraction technique yield a signal of 236 ± 35 events in the data with $Q^2 < 0.26 \text{ GeV}^2/c^2$ and 188 ± 35 events in the data with $0.26 \text{ GeV}^2/c^2 < Q^2 < 1.4 \text{ GeV}^2/c^2$. Attributing all of the events in the signal to the f^0 gives partial widths $\Gamma_{f^0 \rightarrow \gamma\gamma} = 2.0 \pm 0.3 \text{ keV}$ for $Q^2 < 0.26 \text{ GeV}^2/c^2$ and $\Gamma_{f^0 \rightarrow \gamma\gamma} = 1.2 \pm 0.2 \text{ keV}$ for $0.26 < Q^2 < 1.4 \text{ GeV}^2/c^2$. The values of the partial width obtained for the three regions of Q^2 are summarized in Fig. 10. The errors shown in this figure include the statistical uncertainties as well as systematic errors which are not common to the tagged and untagged analyses.

Vector-meson dominance has historically been used to describe the interaction of off-mass shell photons. One generalized vector-dominance model²¹ (GVDM) predicts a shape given by the solid curve in Fig. 10. This curve is normalized to the world average value of 2.8 keV at $Q^2=0$. Basically this model includes contributions from the ρ , ω , and ϕ mesons as well as higher resonances and a continuum. Also included in this GVDM are contributions from the longitudinal-transverse photon combinations. The dotted-dashed curve is the ρ form factor alone

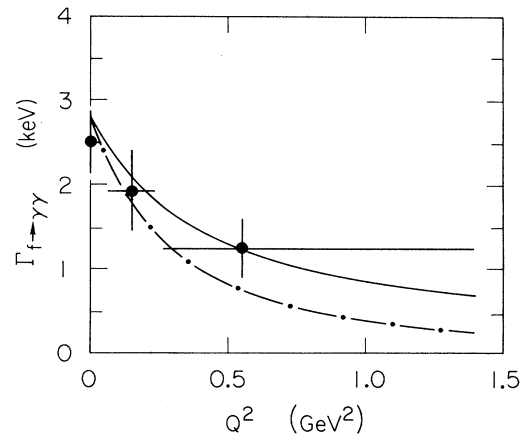


FIG. 10. Measured $\gamma\gamma$ partial width of the $f^0(1270)$ for three bins in Q^2 . The resonance was assumed to be produced in the helicity-2 state in all three cases. The errors shown do not include systematic contributions common to the three parts. The solid curve is a generalized-vector-meson-dominance form factor. The dotted-dashed curve is a simple ρ form factor. These predictions have been normalized at $Q^2=0$ to the value quoted in the Particle Data Group tables.

normalized to the same $Q^2=0$ value. The data tend to prefer the less rapid decrease in Q^2 given by the GVDM of Ref. 21.

An explanation of the data can also be attempted in the framework of the quark model. The nonrelativistic quark model has been used⁴ to calculate the Q^2 dependence of the $\gamma^*\gamma f^0$ vertex. The bound-state problem was treated using a Bethe-Salpeter amplitude for the quark-antiquark amplitude. Essentially an effective "form factor" is calculated from the Bethe-Salpeter amplitude which provides an enhancement over the ρ form factor of about 20% for tagging angles between 24 and 60 mr. This effective form factor is closer to our result than the ρ form factor. Relativistic calculations²² are being performed to improve this model.

In all of the above data analysis, we have assumed that the f^0 is produced in the helicity-2 state. The parton model predicts²³ that, as $Q^2 \rightarrow \infty$, only the helicity-0 amplitude will remain because two photons with spins aligned cannot couple to a quark-antiquark pair in the approximation that the quark mass is zero. This is because the helicity-changing part of the quark current is proportional to the quark mass. Hence, we might expect that there will be a rapid change in the angular distribution as Q^2 is increased from 0 to the asymptotic region (i.e., where scaling sets in). Unfortunately, the region in between is a mixture of helicity states, and the parton model does not provide a clear description. There was not enough data to perform a detailed study of the angular dependence of the production process as a function of Q^2 . The efficiency for detecting an helicity-2 f^0 in the tagged data is approximately twice as large as that for an helicity-0 tagged f^0 event. If we assume that at $Q^2=0$

the f^0 is produced purely in helicity 2 and that at $Q^2=0.6 \text{ GeV}^2/c^2$ the f^0 is produced purely in helicity 0, the difference in detection efficiency is a viable explanation of the data without any further suppression. We would obtain a partial width of $\Gamma_{f^0 \rightarrow \gamma\gamma} = 1.26 \text{ keV}$ at $Q^2=0.6 \text{ GeV}^2/c^2$ (i.e., our data are consistent with a transition from helicity 2 at $Q^2=0$ to helicity 0 at $Q^2=0.6 \text{ GeV}^2/c^2$).

VI. CONCLUSION

We have measured the coupling of the $f^0(1270)$ meson to two real photons and find a partial width $\Gamma_{f^0 \rightarrow \gamma\gamma}$ that is consistent with previous measurements. In addition we have studied the Q^2 dependence of $\Gamma_{f^0 \rightarrow \gamma\gamma}(Q^2)$ and find that it is consistent with a generalized-vector-dominance-model form factor.²¹ The data can also be explained by the nonrelativistic quark model.⁴ In addition the production of two-prong hadron states via the $\gamma\gamma$ interaction is in reasonable agreement with QCD predictions¹ for $\gamma\gamma$ masses $\gtrsim 2.0 \text{ GeV}/c^2$.

ACKNOWLEDGMENTS

We gratefully acknowledge many enlightening discussions with S. J. Brodsky on topics relevant to this work. This work was supported in part by the U.S. Department of Energy under Contracts Nos. DE-AC03-76SF00515 (SLAC), DE-AC03-76SF00098 (LBL), and DE-AC02-76ER03064 (Harvard). Support for individuals also comes from the University of California at Davis and the U.S. National Science Foundation.

^aUniversity of California, Davis, California 95616.

^bPresent address: CERN CH-1211 Geneva 23, Switzerland.

^cPresent address: Argonne National Laboratory, Argonne, Illinois 60439.

^dPresent address: University of Arizona, Tucson, Arizona 85721.

^ePresent address: Xerox Corp., Palo Alto, California 94304.

^fPresent address: Harvard University, Cambridge, Massachusetts 02138.

^gPresent address: University of California at Santa Cruz, Santa Cruz, California 95064.

^hPresent address: California Institute of Technology, Pasadena, California 91125.

ⁱPresent address: Fermilab, Batavia, Illinois 60510.

^jPresent address: University of Massachusetts, Amherst, Massachusetts 01002.

¹S. J. Brodsky and G. P. Lepage, *Phys. Rev. D* **24**, 1808 (1981); *Perturbative Quantum Chromodynamics*, proceedings of the Conference, Tallahassee, 1981, edited by D. W. Duke and J. F. Owens (AIP, New York, 1981), p. 214; *Phys. Rev. D* **22**, 2157 (1980).

²Particle Data Group, *Phys. Lett.* **B111**, 1 (1982).

³R. Brandelik *et al.*, TASSO Collaboration, *Z. Phys. C* **10**, 117 (1981).

⁴H. Krasemann and J. A. M. Vermaseren, *Nucl. Phys.* **B184**, 269 (1981).

⁵Ch. Berger *et al.*, PLUTO Collaboration, *Phys. Lett.* **B94**, 254 (1980).

⁶C. J. Biddick *et al.*, *Phys. Lett.* **B97**, 320 (1980).

⁷A. Roussarie *et al.*, *Phys. Lett.* **B105**, 304 (1981).

⁸R. Schindler, Ph.D. thesis, Report No. SLAC-PUB-265, 1980.

⁹J. A. Jaros, in *Proceedings of the International Conference on Instrumentation for Colliding Beam Physics, Stanford, California, 1981*, edited by W. Ash (Stanford Linear Accelerator Report No. 250, 1982), p. 29.

¹⁰J. R. Smith, Ph.D. thesis, University of California Davis, 1982.

¹¹R. L. Ford and W. R. Nelson, Report No. SLAC-PUB-2107, 1978 (unpublished).

¹²The Monte Carlo simulation used only the σ_{TT} part of the QED cross section [V. M. Budnev *et al.*, *Phys. Rep.* **15**, 181 (1975)]. The QED mass shape is also in agreement with the Smith-Vermaseren Monte Carlo program [J. Smith, J. A. M. Vermaseren, and G. Grammer, *Phys. Rev. D* **15**, 3280 (1977)].

¹³J. M. Blatt and V. F. Weisskopf, *Theoretical Nuclear Physics* (Wiley, New York, 1952), pp. 359–365 and 386–389; we have used Eq. (7.13) for Γ_{tot} normalized to the value 180 MeV at $M = 1.27 \text{ GeV}/c^2$.

¹⁴M. Althoff *et al.*, TASSO Collaboration, *Phys. Lett.* **B121**, 216 (1983).

¹⁵C. Edwards *et al.*, *Phys. Lett.* **B110**, 82 (1982).

- ¹⁶S. J. Brodsky, T. Kinoshita, and H. Terazawa, *Phys. Rev. D* **4**, 1532 (1971).
- ¹⁷F. E. Low, *Phys. Rev.* **120**, 582 (1960).
- ¹⁸G. Bonneau, M. Gourdin, and F. Martin, *Nucl. Phys.* **54B**, 573 (1973).
- ¹⁹D. L. Burke, Report No. SLAC-PUB-2988, 1982 (unpublished); in *Proceedings of the 21st International Conference on High Energy Physics, Paris, 1982*, edited by P. Petiau and M. Porneuf [*J. Phys. (Paris) Colloq.* **43**, C3-513 (1982)].
- ²⁰J. H. Field, *Nucl. Phys.* **B168**, 477 (1980).
- ²¹I. F. Ginzburg and V. G. Serbo, *Phys. Lett.* **B109**, 231 (1982).
- ²²L. Bergström, G. Hulth, and H. Snellman, Report No. REF. TH. 3381-CERN, 1982 (unpublished).
- ²³G. Köpp, T. F. Walsh, and P. Zerwas, *Nucl. Phys.* **B70**, 461 (1974).